Enhanced Simulated Sun Light Photocatalytic Activity of α-Fe_2O_3 Modified g-C_3N_4 prepared In-situ

Xinlu Liu[1], Junbo Zhong[1], Jianzhang Li*[, 1], Wei Hu[1], Qizhao Wang[2], Guangbin Wang[1], Jiabo Song[1], Ke Liu[1], Ke Huang[1], Songlin Wu[1], Ruhao Yang[1], Minjiao Li[3]

[1]Key Laboratory of Green Catalysis of Higher Education Institutes of Sichuan, College of Chemistry and Pharmaceutical Engineering, Sichuan University of Science and Engineering, Zigong, 643000, P R China
[2]College of Chemistry and Chemical Engineering, Northwest Normal University, Lanzhou 730070, PR China
[3]College of Materials and Chemical Engineering, Sichuan University of Science and Engineering, Zigong, 643000, PR China

Abstract:

In this paper, α-Fe_2O_3/g-C_3N_4 composite photocatalysts were fabricated in-situ by a facile hydrothermal method and characterized by Brunauer-Emmett-Teller (BET) method, X-ray diffraction (XRD), scanning electron microscopy (SEM), UV/Vis diffuse reflectance spectroscopy (DRS), transmission electron microscopy (TEM), X-ray photoelectron spectroscopy (XPS) and surface photovoltage spectroscopy (SPS), respectively. The photocatalytic activity of α-Fe_2O_3/g-C_3N_4 for decolorization of methyl orange (MO) aqueous solution was evaluated. The results show that α-Fe_2O_3/g-C_3N_4 composites exhibit higher photocatalytic performance than the pure g-C_3N_4 under simulated sun light irradiation. The remarkably increased performance of α-Fe_2O_3/g-C_3N_4 in photocatalysis could be attributed to the increased specific surface area, the enhanced light absorbance, the improved separation efficiency of photo-induced charge carriers and the strong interaction between α-Fe_2O_3 and g-C_3N_4. The enhanced mechanism was proposed and proven by SPS analysis.

Keywords: g-C_3N_4; α-Fe_2O_3; heterojuctions; photocatalytic performance; Mechanism

Introduction

Since the first report by Wang *et al*. that graphitic carbon nitride (g-C_3N_4) possessed good visible-light-driven photocatalytic performance and could produce hydrogen or oxygen by water splitting under visible light (1), g-C_3N_4 has attracted increasing research interest as a promising visible light photocatalyst owing to its unique structure and electronic properties (1, 2-6). g-C_3N_4 has a smaller direct band gap due to the sp^2 hybridization of carbon and nitrogen forming the π-conjugated graphitic planes (7). The bandgap energy of g-C_3N_4 is about 2.7 eV, the conduction band (CB) and the valence band (VB) of g-C_3N_4 is -1.3 V and 1.4 V at pH 7.0 vs the normal hydrogen electrode (NHE), respectively (8, 9).

However, the photocatalytic activity of g-C_3N_4 is far from efficient due to the quick recombination of the carriers (10); therefore, it is crucial to promote the photocatalytic performance. Continuous attempts have been developed to boost the photocatalytic activity of g-C_3N_4, such as the choice of preparation method (11-13), doping (14-16) and construction of composite photocatalysts (17-22). Among these approaches, construction of heterojuctions with matching band potentials is an effective way to improve the photocatalytic activity. Heterojuctions can promote the separation efficient of the photo-induced charge carriers due to the different band potentials and work function, resulting in high photocatalytic performance.

As an n-type semiconductor, hematite (α-Fe_2O_3) is one of promising and cheapest photocatalysts due to its outstanding advantages (23-28), such as narrow band gap (about 2.20 eV), low cost and nontoxic. Y. Lv and coworkers prepared α-Fe_2O_3/g-C_3N_4 composites by a facile refluxing method, the results show that α-Fe_2O_3/g-C_3N_4 displays highly catalytic and distinctly selective for detection H_2S gas (29). However, few studies have been reported on the activity of α-Fe_2O_3/g-C_3N_4 composites prepared in-situ under simulated solar irradiation, especially the photo-induced charge separation efficiency.

In this work, the α-Fe_2O_3/g-C_3N_4 composites were fabricated in situ by a facile hydrothermal method and characterized by BET, XRD, SEM/TEM, DRS and SPS. The effects of Fe_2O_3 loading on the structure, surface texture, response to light, the photo-induced charge separation efficiency and their relation with the photocatalytic activity of α-Fe_2O_3/g-C_3N_4 were

*Corresponding author; E-mail address: scuzhong@sina.com

discussed. The photocatalytic activities of the as-prepared samples were investigated by decolorization of methyl orange (MO) aqueous under simulated sun light irradiation. The α-Fe_2O_3/g-C_3N_4 photocatalysts exhibit much higher photocatalytic activity than the pure g-C_3N_4, which is attributed to the heterostructure between g-C_3N_4 and α-Fe_2O_3, resulting in high separation rate of photo-induced charge carriers. In addition, the possible photocatalytic mechanism was proposed.

Experimental Section

Preparation of Photocatalysts

All reagents were purchased from Chengdu Kelong Chemical Reagents Factory and used as received. All the studies were done using deionized water and reagents of A.R grade. g-C_3N_4 was prepared by heating melamine in a muffle furnace. 20.0 g of melamine was put into an alumina crucible with a cover, and then baked in air at 823K for 3 h. After cooled to room temperature, the resulted yellow product was collected and ground into powder. The α-Fe_2O_3/g-C_3N_4 composites were fabricated in situ by a facile hydrothermal method. 2g g-C_3N_4 was dispersed in 20 mL deionized water by ultrasonic for 10 min, then 10 mL $FeCl_3$ aqueous solution was added dropwise to g-C_3N_4 under intense stirring (The molar ratio of Fe/g-C_3N_4 is 0%, 1%, 2%, 3% and 4%, respectively). The mixture mentioned above was transferred into a 50 mL Teflon-lined stainless-steel autoclave. The autoclave was maintained at 453K for 24 h and then cooled to room temperature naturally. The resulting product was collected by filtration, washed with deionized water until no Cl^- could be detected (using Ag^+), and then dispersed in absolute ethanol and dried at 333K in air overnight. α-Fe_2O_3/g-C_3N_4 samples prepared with different initial molar ratios of Fe/g-C_3N_4 (0%, 1%, 2%, 3% and 4%) were named as 0% (g-C_3N_4), 1%, 2%, 3% and 4%, respectively.

Characterization of the Photocatalysts

The specific surface area measurements were performed on a SSA-4200 automatic surface analyzer (Builder, China). X-ray diffraction (XRD) patterns were recorded on a DX-2600 X-ray diffractometer using Cu Kα (λ=0.15406 nm) radiation and equipped with a graphite monochromator. The X-ray tube was operated at 40 kV and 25 mA. Samples were scanned from 2θ equal to 10° up to 90° and the X-ray diffraction line positions were determined with a step size of 0.03° and a slit of 1. The UV-Vis spectra of photo-catalysts in the 300-850 nm range were recorded using a TU-1907 UV-Vis spectrophotometer equipped with an integrating sphere, and $BaSO_4$ was used as the reference. SEM images were taken with a JSM-7500F scanning electron microscope, using an accelerating voltage of 5 kV. Before SEM measurement, the sample was dispersed in water assisted by ultrasonic for 10 min and then gold plating was performed. Transmission electron microscopy (TEM) was recorded on a Philips Fei Tecnai Sprit electron microscope at an accelerating voltage of 120 kV. X-ray photoelectron spectroscopy (XPS) measurements were performed on a XSAM 800 using Mg Kα at 12 kV and 12 mA. The X-ray photoelectron spectra were referenced to the C1s peak (*BE*=284.80 eV) resulting from adventitious hydrocarbon (i.e. from the XPS instrument itself) present on the sample surface. The measurements of surface photovoltage spectroscopy (SPS) were carried out according to the procedure described in reference (35, 36). The real content of Fe on g-C_3N_4 was measured by Fe^{2+}-1,10-Phenanthroline spectrophotometric method.

Evaluation of the Photocatalytic Activity

The measurements of photocatalytic activity were performed in a Phchem Ⅲ photochemical reactor (Beijing NBET Technology Co., Ltd, China) under intense stirring. In a typical photocatalytic experiment, 50 mg of photocatalyst was added into 50 mL MO aqueous solution (10 mg/L). The light source was a 350 W Xe lamp (simulated sun light), the lamp was encapsulated in a cooling quartz jacket and positioned in the middle of the reactor. Quartz test tubes were located around the lamp and the distance from the lamp to the quartz test tubes was 10 cm. The decolorization reaction was performed at room temperature. The pH value of the reaction solution was 7.0. After 2h, the samples were removed and centrifuged (9000 rpm) to separate the photocatalyst for analysis. The concentration of MO was measured by a 756 PC spectrophotometer at 460 nm and analyzed by Lambert-Beer law. To detect the related reactive species, hydroxyl radicals (•OH), superoxide radicals ($\bullet O_2^-$) and holes (h^+) were investigated by adding isopropanol (IPA), benzoquinone (BQ) and ammonium oxalate (AO) into the MO solution, respectively (37-39). The experiment was similar to the photocatalytic decolorization experiment.

Results and Discussion

Characterization of photocatalysts

Table 1 shows the specific surface parameters of photocatalysts with different loading of Fe_2O_3. The highest specific surface area and pore volume, and the smallest pore size is obtained when Fe loading is

Table 1. Parameters of photocatalysts

Catalysts	SBET (m^2/g)	Pore volumes (cc/g)	Pore size (nm)	molar ratio of Fe/g-C_3N_4
0%	8.7	0.0046	10.8	0%
1%	9.5	0.0047	10.0	0.145%
2%	11.9	0.0064	9.2	0.171%
3%	21.7	0.0107	7.8	0.193%
4%	13.1	0.0070	8.8	0.237%

about 0.193 mol%, then the specific surface area and pore volume drops at about 0.237 mol%. It is interesting to notice that the specific surface area of 0.193%Fe is 2.5 times of that of pure g-C_3N_4. The results indicate that a low content of Fe_2O_3 can increase the specific surface area of photocatalyst, while a relative large amount of Fe_2O_3 may nucleate on the surface of g-C_3N_4 due to the limited specific surface area of g-C_3N_4, resulting in low specific surface area and pore volume. It is commonly accepted that the performance of the catalyst can be benefited from the high surface area, providing a large number of adsorption sites. The results can be further confirmed by the results of adsorption measurements.

The XRD patterns of the samples are shown in Figure 1. The diffraction peaks of g-C_3N_4 and Fe_2O_3/g-C_3N_4 composites can be indexed to the single phase. For Fe_2O_3/g-C_3N_4 composites, no peaks of Fe_2O_3 were detected by XRD in the 2θ region from 20^0 to 70^0. We believe this could be attributed to two factors: 1) the loaded Fe_2O_3 is highly dispersed on the support matrix, and 2) the percentage of Fe_2O_3 is very low, which can be confirmed by the results in Table1. Furthermore, it is interesting that the full width at half maximum (FWHM) of 1%, 2%, 3% and 4% is wider than that of g-C_3N_4. According to Scherrer equation, the wider the FWHM is, the smaller the crystal size of g-C_3N_4 is. This result demonstrates that the increased crystal size leads to the BET surface area decrease, which fits well with the result of BET surface area. Furthermore, for 2% and 3% sample, there is a shift in the peak position of g-C_3N_4, indicating a strong interaction exists between Fe_2O_3 and g-C_3N_4. For Fe_2O_3, the two peaks located at 33.25^0 and 35.68^0 match well with the (104) and (110) planes of α-Fe_2O_3, as evidenced from the PXRD pattern (JCPDS No.33-0664).

It is now commonly recognized that the band gap can be adjusted effectively by combining two kinds of semiconductor photocatalysts, promoting the photocatalytic activity. As shown in Figure 2, loading of α-Fe_2O_3 onto the surface of g-C_3N_4 enlarges the light absorption range of the composite photocatalysts, since the bandgap of α-Fe_2O_3 is around 2.2 eV. The

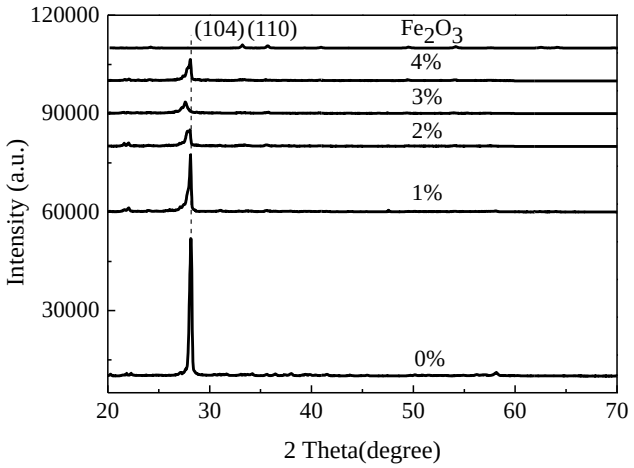

Figure 1. XRD patterns of photocatalysts.

indirect bandgap of the samples was measured by fitting to a plot of $(\alpha h\nu)^2$ versus hν, where α is absorbance. Due to partial overlap of curves of α-Fe_2O_3/g-C_3N_4, only the values of α-Fe_2O_3, g-C_3N_4 and 3% are shown in Figure 3. The indirect bandgap for α-Fe_2O_3, g-C_3N_4 and 3% is 2.20, 2.85 and 2.53 eV, respectively. The results indicate that the composites exhibit improved absorption ability in the visible light range in the presence of α-Fe_2O_3, which suggests that the photocatalytic activity can be greatly increased by the effective absorption of visible light compared with pure g-C_3N_4. This result agrees well with the results of the photocatalytic activity measurements. For g-C_3N_4, the band gap is 2.85 eV, which matches the value (2.70-3.0 eV) reported by Zhu and coworkers (12).

The SEM images and TEM of photocatalysts prepared are shown in Figure 4. As shown in Figure 4, α-Fe_2O_3 is irregular bar and lump-like morphology, and g-C_3N_4 is irregular lump and honeycomb-like morphology, for 3% sample, bars of α-Fe_2O_3 were observed on the surface of g-C_3N_4. Furthermore, the shape of g-C_3N_4 for 3% sample is different from the SEM images of the pure g-C_3N_4. The change of the morphology of g-C_3N_4 is due to the presence of the precursor of α-Fe_2O_3 during the preparation. The TEM shows that α-Fe_2O_3 is on the surface of g-C_3N_4.

Figure 5 shows the high resolution XPS spectra for Fe 2p, the XPS spectra show no elemental Fe

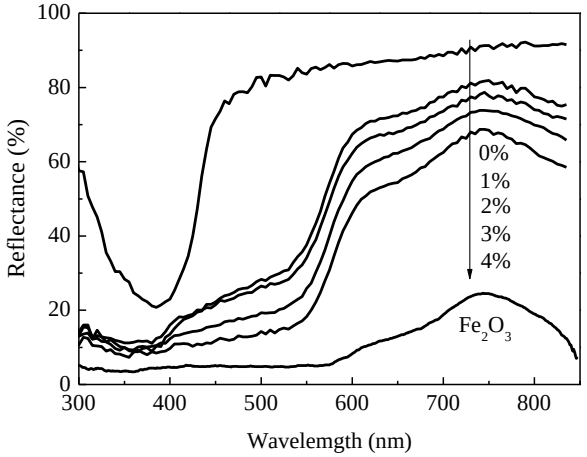

Figure 2. UV-Vis diffuse reflectance spectra of photocatalysts.

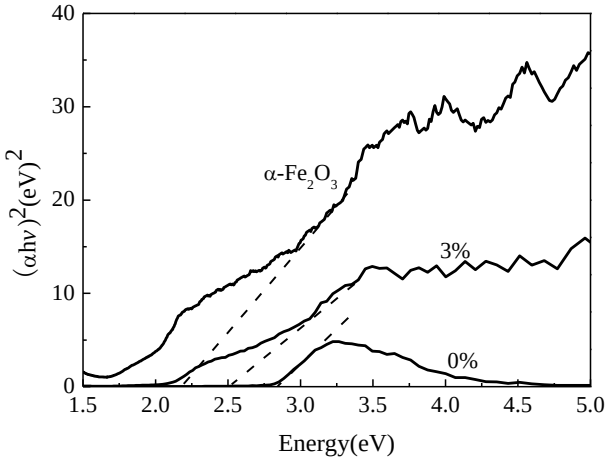

Figure 3. Plot of $(\alpha h\nu)^2$ and hν.

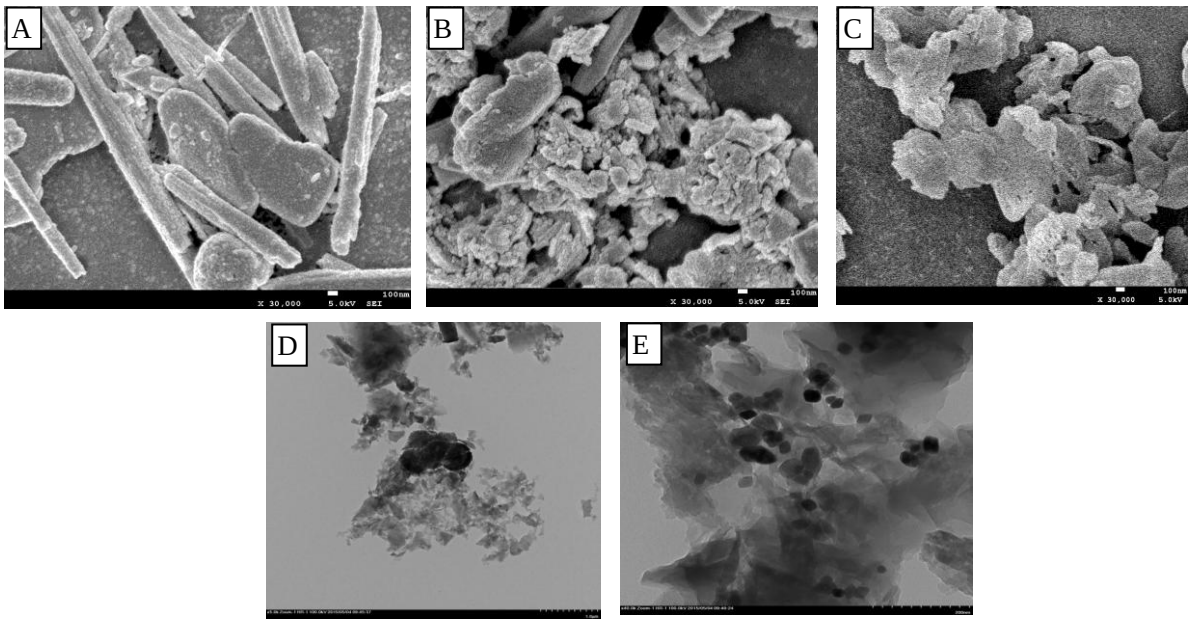

Figure 4. (A, B, C) SEM and (D, E) TEM images of photocatalysts; (A) α-Fe_2O_3; (B) 3%; (C) g-C_3N_4; (D) g-C_3N_4; (E) 4%.

peak, which indicates that the element Fe in Fe_2O_3/g-C_3N_4 composites exists in the oxide state only. The peak occurs at around 710.8 eV is assigned to Fe $2p_{3/2}$ of Fe_2O_3 (29, 40), demonstrating the existence of Fe^{3+} in the composites. However, Fe $2p_{3/2}$ of 3% and 4% shifts to lower value compare to the 710.8 eV, suggesting a strong interaction between g-C_3N_4 and Fe_2O_3 exists. The results of Table 1, XRD, TEM and XPS suggest that heterostructures are composed of α-Fe_2O_3 and g-C_3N_4.

The SPS responses of g-C_3N_4 and α-Fe_2O_3/g-C_3N_4 composites are shown in Figure 6. It can be seen that g-C_3N_4 displays obvious SPS response from 300-400 nm and 400-500 nm, respectively, which is attributed to the electronic transitions from the VB to CB according to the DRS spectra and energy band structure of g-C_3N_4. As shown in Figure 6, the SPS response of α-Fe_2O_3/g-C_3N_4 in UV and visible light region gradually increases as the loading of α-Fe_2O_3 increasing, and reaches the maximum at 3%, then drops dramatically at 4%. Generally, the strong SPS response corresponds to the high separation rate of photo-induced charge (35, 36), thus, the 3% sample holds the highest charge separation rate among the experimented compositions, while 0% sample has the lowest charge separation rate. Among all the factors that affect the photocatalytic performance, the number of photo-generated charge carriers plays an important role in influencing the photocatalytic activity: the more the number of carriers, the better the photo-catalyst (41). High photocatalytic activity can be benefited from the high rate of charge separation; this result fits well with the photocatalytic performance measurements.

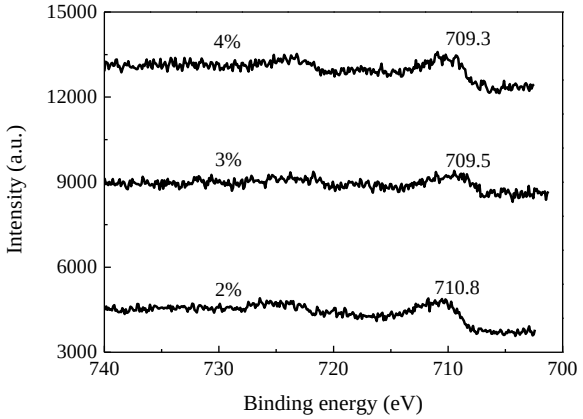

Figure 5. High resolution XPS spectra of the Fe 2p on the surface of photocatalysts.

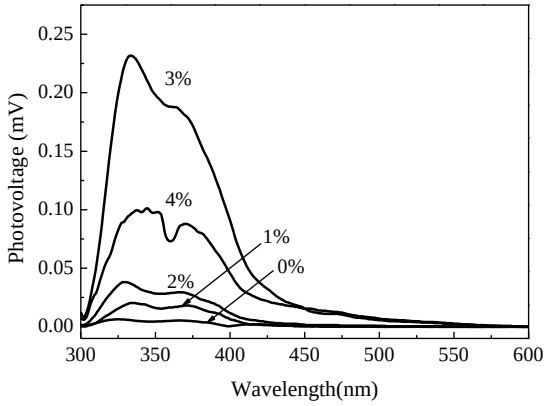

Figure 6. SPS of photocatalysts.

Photocatalytic Activity and Mechanism

The photolysis of MO aqueous solution (10 mg/L) under simulated solar irradiation without photocatalyst after 2 h is so small that can be totally ignored, the adsorption of MO on different photocatalysts after 2h in a dark is shown in Figure 7. The results illustrate that the adsorption of MO tends to increase upon loading of α-Fe_2O_3, the increased adsorption of MO favors the photocatalytic activity of catalyst. Among these five photocatalysts, 3% sample has the highest adsorption toward MO, the value is 9.5%; however, a large amount of α-Fe_2O_3 loading is harmful for the adsorption possibly due to the coverage of g-C_3N_4 active sites. The change tendency of adsorption of MO on photocatalysts fits well with the performance of photocatalysts.

The photocatalytic activities of g-C_3N_4 and α-Fe_2O_3/g-C_3N_4 are shown in Figure 8. As shown in Figure 8, all α-Fe_2O_3/g-C_3N_4 photocatalysts exhibit better photocatalytic activity than g-C_3N_4 and the 3% sample exhibits the best photocatalytic activity among the experimented compositions. The results show that the lower α-Fe_2O_3 loading exhibits better performance due to higher dispersion of α-Fe_2O_3 on the surface of

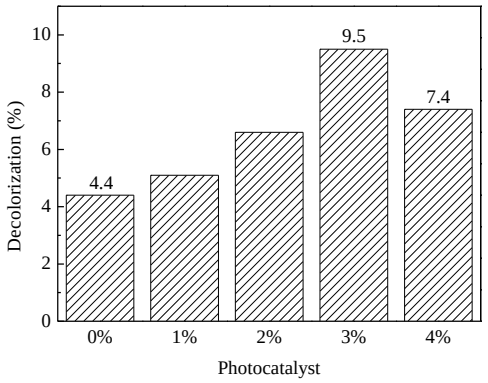

Figure 7. Adsorption of MO on the different photocatalysts after 2h in dark.

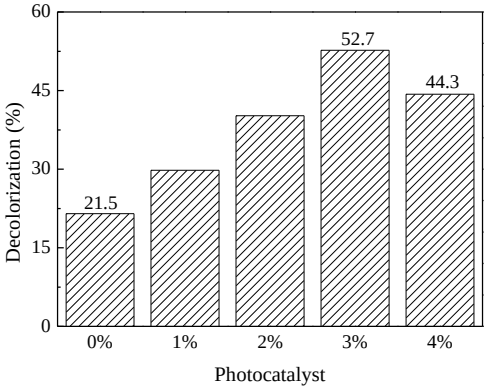

Figure 8. Decolorization of MO over photocatalysts for 2h.

g-C_3N_4, however, relative high content of α-Fe_2O_3 is harmful for the activity possibly due to the coverage of g-C_3N_4 active sites by α-Fe_2O_3, resulting in low separation rate of photo-induced charge and specific surface area, thus activity of 4% is worse than that of 3%.

To detect the reactive species in photocatalytic process, the effects of three scavengers on the photocatalytic decolorization of MO were investigated. Usually, as a consequence of quenching, photocatalytic decolorization of MO will be lower. The more MO decolorization efficiency is decreased by a scavenger, the more important role the corresponding reactive species plays in the photocatalytic reaction. The effects of three scavengers on the photocatalytic decolorization of MO are shown in Figure 9. The photocatalytic decolorization efficiency of MO drops obviously from 52.7% to 23.5% after adding BQ, indicating that $\bullet O_2^-$ is the main active species in the photocatalytic decolorization process. When AO is added, the photocatalytic decolorization of MO drops to 40.3%, which indicates that h^+ plays the secondary important role in the oxidation of MO. When IPA is added, the photocatalytic decolorization of MO is 50.2%, considering the measurement error, no •OH exists in the photocatalytic process.

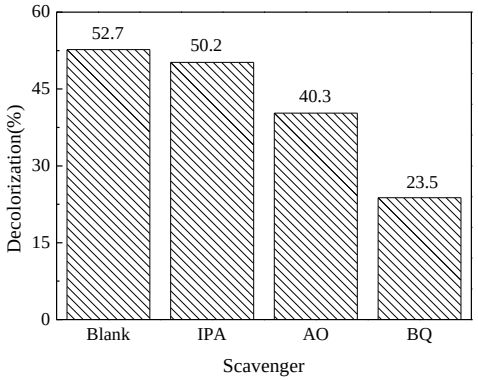

Figure 9. Effects of scavengers on the decolorization efficiency of MO over 3% sample (Illumination time= 2h, Scavenger dosage= 0.2 mmol/L).

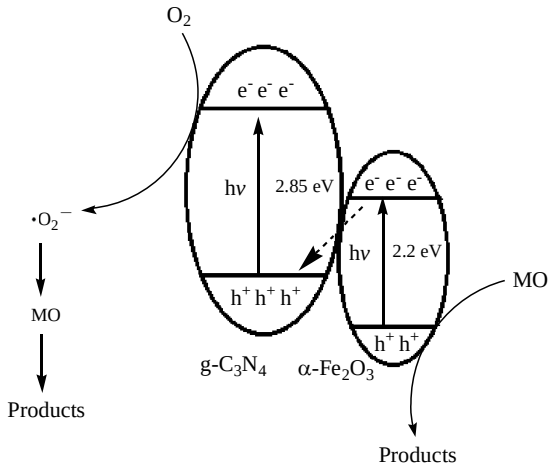

Figure 10. Schematic diagram of the separation and transfer of photogenerated charges in the α-Fe_2O_3/C_3N_4 heterojunctions.

On the basis of the above results, a possible mechanism for the photocatalytic activity enhancement of α-Fe_2O_3/g-C_3N_4 heterojuctions is proposed in Figure 10. Compared the VB potential of g-C_3N_4 with the standard redox potential of OH^-/•OH (1.99 V *vs.* NHE), the VB potential of g-C_3N_4 is more negative than the standard redox potential of OH^-/•OH, and therefore h^+_{VB} cannot oxidize OH^- to generate •OH radicals directly in photocatalytic reaction system. The CB and VB of α-Fe_2O_3 are 0.34 V and 2.55 V (vs. NHE) (33), respectively. At pH 7.0, the standard redox potential of H_2O/·OH is about 2.7~2.8 eV, thus h^+_{VB} on VB of α-Fe_2O_3 cannot oxidize H_2O to generate •OH. Similarly, the electrons on CB of α-Fe_2O_3 cannot produce $\bullet O_2^-$ from dissolved O_2 by the photoreduction process since the conduction edge potential is more positive than the standard redox potential E^0 (O_2/$\bullet O_2^-$) (−0.3 V vs. NHE). The redox potentials of both the conduction band and valence band of g-C_3N_4 are more negative than those of the conduction band and the valence band of α-Fe_2O_3. Under visible light, the photo-induced electrons with low reductive power in the CB of α-Fe_2O_3 transfer to the VB of g-C_3N_4 quickly, resulting in the combination of these electrons with photo-induced holes with low oxidative power of g-C_3N_4, thus the accumulated rich electrons in the CB of g-C_3N_4 and holes in the VB of α-Fe_2O_3 can take part in the reduction and oxidation reactions, respectively. It is clear that the charge carrier transfer is not the common model (i.e. transfer of electrons from CB of g-C_3N_4 to CB of α-Fe_2O_3). According to Figure 10, the electrons in the CB of g-C_3N_4 have more negative potential to reduce the molecular oxygen to yield $\bullet O_2^-$. The holes in the valance band of α-Fe_2O_3 play an important in decolorization of MO. According to the results, a direct Z-scheme mechanism was suggested for the effective separation process of photo-induced electron–hole pairs. In fact, a similar Z-scheme mechanism for g-C_3N_4/N-doped $SrTiO_3$ and g-C_3N_4/AgBr composite photocatalysts has been reported by some researchers (42, 43).

In this work, 3% sample has the highest photocatalytic performance. We attributed this improvement to the enhanced specific surface parameters, high separation rate of photo-induced charge carriers, and the strong interaction between α-Fe_2O_3 and g-C_3N_4. Also, the facile synthesis method may be useful for constructing other heterojuctions.

Conclusions

In summary, α-Fe_2O_3 modified g-C_3N_4 photocatalysts were synthesized in-situ by a facile hydrothermal method. The as-prepared α-Fe_2O_3/g-C_3N_4 composites exhibit higher photocatalytic activities in decolorization of methyl orange aqueous solution under simulated solar illumination than g-C_3N_4. The α-Fe_2O_3 (3%Fe)/g-C_3N_4 sample has the highest photocatalytic activity for MO decolorization. The remarkably increased performance of α-Fe_2O_3/g-C_3N_4 could be attributed to the increased specific surface area, the enhanced light absorbance, the improved separation efficiency of photo-induced charge carriers and the strong interaction between α-Fe_2O_3 and g-C_3N_4.

Acknowledgements

This project was supported financially by the program of Science and Technology Department of Sichuan province (No.2013JY0080, No.2015JY0081), Students Innovation Project of Sichuan Province (No.201410622003), Research Fund Projects of Sichuan University of Science and Engineering (No.2013PY03), the Project of Zigong city (No. 2014HX14), Construct Program of the Discipline in Sichuan University of Science and Engineering and the Opening Project of Key Laboratory of Green

Catalysis of Sichuan Institutes of High Education (No.LZJ1302).

References

(1) Wang, X.C.; Maeda, K.; Thomas, A.; Takanabe, K.; Xin, G.; Carlsson, J.M.; Domen, K.; Antonietti, M. *Nat. Mater*. **2009**, *8*, 76-80.

(2) Gong,Y.T.; Li, M.M.; Li, H.R.; Wang, Y. *Green Chem.* **2015**, *17*, 715-736.

(3) Zheng, Y.; Liu, J.; Liang, J.; Jaroniecc, M.; Qiao, S.Z. *Energy Environ. Sci*. **2012**, *5*, 6717 -6731.

(4) Fan, X.Q.; Xing, Z.; Shu, Z.; Zhang, L.X.; Wang, L.Z.; Shi, J.L. *RSC Adv*. **2015**, *5*, 8323-8328.

(5) Niu, P.; Zhang, L.L.; Liu, G.; Cheng, H.M. *Adv. Funct. Mater*. **2012**, *22*, 4763-4770.

(6) Cao, S. W.; Yu, J. G. *J. Phys. Chem. Lett*. **2014**, *5*, 2101-2107.

(7) Thomas, A.; Fischer, A.; Goettmann, F.; Antonnietti, M.; Muller, J.O.; Schlogl, R.; Carlsson, J.M. *J. Chem. Mater*. **2008**, *18*, 4893-4908.

(8) Wang, Y.; Wang, X.; Antonietti, M. Angew. *Chem., Int. Ed*. **2012**, *51*, 68-89.

(9) Su, F.Z.; Mathew, S.C.; Lipner, G.; Fu, X.Z.; Antonietti, M.; Blechert, S.; Wang, X.C. *J. Am. Chem. Soc*. **2010**, *132*, 16299-16301.

(10) Hou, Y.; Wen, Z.; Cui, S.; Guo, X.; Chen, J. *Adv. Mater*. **2013**, *25*, 6291-6297.

(11) Yuan, B.; Chu, Z.Y.; Li, G.Y.; Jiang, Z.H.; Hu, T.J.; Wang, Q.H.; Wang, C.H. *J. Mater. Chem. C*. **2014**, *2*, 8212-8215.

(12) Bai, X.J.; Yan, S.C.; Wang, J.J.; Wang, L.; Jiang, W.J.; Wu, S.L.; Sun, C.P.; Zhu, Y.F. *J. Mater. Chem. A*. **2014**, *2*, 17521-17529.

(13) Huang, Z.J.; Li, F.B.; Chen, B.F.; Yuan, G.Q. *Catal. Sci. Technol*. **2014**, *4*, 4258-4264.

(14) Ge, L.; Han, C.C.; Xiao, X.L.; Guo, L.L.; Li, Y. *J. Mater. Res. Bull*. **2013**, *48*, 3919-3925.

(15) Zhang, L.G.; Chen, X.F.; Guan, J.; Jiang, Y.J.; Hou, T.G.; Mu, X.D. *Mater. Res. Bull*. **2013**, *48*, 3485-3491.

(16) Hu, H.Z.; Ma, L.; You, J.G.; Li, F.Y.; Fan, Z.P.; Lu, G.; Liu, D.; Gui, J.Z. *Appl. Surf. Sci*. **2014**, *311*, 164-171.

(17) Huang, Z.A.; Sun, Q.; Lv, K.L.; Zhang, Z.H.; Li, M.; Li, B. *Appl. Catal. B: Environ*. **2015**, *164*, 420-427.

(18) Katsumata, H.; Sakai, T.; Suzuki, T.; Kaneco, S. *Ind. Eng. Chem. Res*. **2014**, *53*, 8018-8025.

(19) Feng, Y.; Shen, J.C.; Cai, Q.F.; Yang, H.; Shen, Q.H. *New J. Chem*. **2015**, *39*, 1132-1138.

(20) Yan, T.; Yan, Q.; Wang, X.D.; Liu, H.Y.; Li, M. M.; Lu, S.X.; Xu, W.G.; Sun, M. *Dalton Trans*. **2015**, *44*, 1601-1611.

(21) Cao, S.W.; Yuan, Y.P.; Barber, J.; Loo, S.C.J.; Xue, C. *Appl. Surf. Sci*. **2014**, *319*, 344-349.

(22) Akhundi A.; Habibi-Yangjeh, A. *Ceram. Int*. **2015**, *4*, 5634-5643.

(23) Hu, Y.S.; Shwarsctein, A.K.; Forman, A.J.; Hazen, D.; Park, J.N.; McFarland, E.W. *Chem. Mater*. **2008**, *20*, 3803-3805.

(24) Cesar, I.; Kay, A.; Martinez, J.A.G.; Gratzel, M. *J. Am. Chem. Soc*. **2006**, *128*, 4582-4583.

(25) Zhong, D.K.; Sun, J.W.; Inumaru, H.; Gamelin, D.R. *J. Am. Chem. Soc*. **2009**, *131*, 6086-6087.

(26) Chueh, Y.L.; Lai, M.W.; Liang, J.Q.; Chou, L.J.; Wang, Z.L. *Adv. Funct. Mater*. **2006**, *16*, 2243-2251.

(27) Umar, A.; Abaker, M.; Faisal, M.; Hwang, S.W.; Baskoutas, S.; Al-Sayari, S.A. *J. Nanosci. Nanotechnol*. **2011**, *11*, 3474-3480.

(28) Spray, R.L.; McDonald, K.J.; Choi, K.S. *J. Phys. Chem. C*. **2011**, *115*, 3497-3506.

(29) Zeng, B.R.; Zhang, L.C.; Wan, X.Y.; Song, H.J.; Lv, Y. *Sensor. Actuat. B: Chem*. **2015**, *211*, 370-376.

(30) Donchev, V.; Kirilov, K.; Ivanov, T.; Germanova, K. *Mat. Sci. Eng. B*. **2006**, *129*, 186-192.

(31) Lin, Y.H.; Wang, D.J.; Zhao, Q.D.; Yang, M.; Zhang, Q.L. *J. Phys. Chem. B*. **2004**, *108*, 3202-3206.

(32) Meng, S.G.; Li, D.Z.; Sun, M.; Li, W.J.; Wang, J.X.; Chen, J.; Fu, X.Z.; Xiao, G.C. *Catal. Commun*. **2011**, *12*, 972-975.

(33) Zhang, L.S.; Wong, K.H.; Yip, H.Y.; Hu, C.; Yu, J.C.; Chan, C.Y.; Wong, P.K. *Environ. Sci. Technol*. **2010**, *44*, 1392-1398.

(34) Yin, M.C.; Li, Z.S.; Kou, J.H.; Zou, Z.G. *Environ. Sci. Technol*. **2009**, *43*, 8361-8366.

(35) Kronik, L.; Shapira, Y. *Surf. Sci. Rep*. **1999**, *254*, 1-205.

(36) Jing, L.Q.; Wang, J.; Qu, Y.; Luan, Y. *Appl. Surf. Sci.* **2009**, *256*, 657-663.

(37) Meng, S.G.; Li, D.Z.; Sun, M.; Li, W.J.; Wang, J.X.; Chen, J.; Fu, X.Z.; Xiao, G.C. *Catal. Commun*. **2011**, *12*, 972-975.

(38) Zhang, L.S.; Wong, K.H.; Yip, H.Y.; Hu, C.; Yu, J.C.; Chan, C.Y.; Wong, P.K. *Environ. Sci. Technol*. **2010**, *44*, 1392-1398.

(39) Yin, M.C.; Li, Z.S.; Kou, J.H.; Zou, Z.G. *Environ. Sci. Technol.* **2009**, *43*, 8361-8366.

(40) Yamashita, T.; Hayes, P. *Appl. Surf. Sci*. **2008**, *254*, 2441-2449.

(41) Lu, Y., Lin, Y.; Wang, D.; Wang, L.; Xie, T.; Jiang, T. *Nano Res*. **2011**, *4*, 1144-1152.

(42) Kumar, S.; Tonda, S.; Baruah, A.; Kumarb, B.; Shanker, V. *Dalton Trans*. **2014**, *43*, 16105-16114.

(43) Feng, Y.; Shen, J.; Cai, Q.; Yang, H.; Shen, Q. *New J. Chem*. **2015**, *39*, 1132-1138.

Received for review March 4, 2015. Revised manuscript received June 1, 2015. Accepted June 2, 2015.